IEEE Access
Multidisciplinary ⋮ Rapid Review ⋮ Open Access Journal

Received 3 May 2024, accepted 30 May 2024, date of publication 4 June 2024, date of current version 14 June 2024.

*Digital Object Identifier 10.1109/ACCESS.2024.3409531*

RESEARCH ARTICLE

# The Optimal Design and an Analysis of a Hybrid W-Shaped IPM Rotor of Coaxial Magnetic Gear

**MOHAMMAD AMIN MASOUDI AND SEYED AHMADREZA AFSARI**
Department of Electrical and Computer Engineering, University of Kashan, Kashan 8731753153, Iran
Corresponding author: Seyed Ahmadreza Afsari (afsari@kashanu.ac.ir)

**ABSTRACT** This paper presents a hybrid, W-shaped interior permanent magnet (HWIPM) rotor of a coaxial magnetic gear (MG). To reduce the usage of rare-earth PM material, it proposes a topology of inner rotor in a MG with two types of PM materials. The key point about this idea is that NdFeB PM is applied in combination with ferrite PM to form a hybrid PM excitation. This new type of HWIPM rotor is introduced, and the structure and principles of the operation are explained in details. The optimization and analysis results, using finite element method, showed that this structure could improve torque density and reduce cogging torque, while the cost of rare-earth PM consumption decreased, compared with conventional flat type interior PM-MG. A prototype was fabricated and the performances were experimentally verified. The experimental results showed that the proposed MG had superiorities of low cogging torque, low PM cost, and high torque density compared with conventional coaxial MGs.

**INDEX TERMS** Magnetic gear, hybrid IPM rotor, rare-earth PM, torque density, cogging torque, FEM.

## I. INTRODUCTION

Mechanical gears are widely used to match speed and torque in industrial applications. Compared with mechanical gears, magnetic gears (MGs) have advantages such as low acoustic noise, low vibration, reduced maintenance, and inherent overload protection [1], [2]. These features have attracted further attention and investigation into MGs. Among different MG topologies, coaxial MGs, as radial flux topology, are introduced widely due to the ease of construction and application [3]. The compound motor composed of MG and motor is widely used in the field of low-speed (LS) and high-torque transmission, especially in wind power generation and electric vehicles [4], [5], [6]. As shown in Fig. 1, coaxial MG, generally composes of three different rotors. Permanent magnets (PMs) are mounted on (or buried inside) both the inner and outer cores; soft magnetic pole pieces (flux modulators) are placed between these two rotors. The cores of both rotors and modulators are composed of soft magnetic steel laminations [7], [8], [9], [10], [11]. Magnetic field of PM rotor modulates by passing through the pole pieces. The highest magnitude, modulating harmonic, couples magnetically with another PM rotor to rotate it in a different speed. PM placement in an inner high-speed rotor requires considerations that should be taken into account in the design procedure.

Generally, PM machines can be categorized as surface-mounted PM (SPM) and interior PM (IPM) topologies. The SPM machines are generally known for having large air gap, small saliency ratio, equally direct, and quadrature axis inductance, whereas the IPM machines are generally known for non-salient structure, small air gap, large saliency ratio, variation in direct, and quadrature axis inductance [12], [13]. The high rotational speed of an inner rotor in MGs forces the use of IPM type. Due to a limited space in placing PMs in IPM structures, V-shaped IPM structures are introduced. These topologies present a higher saliency ratio and higher PM surface compared with the flat-types, making it more suitable for high-speed applications [14], [15].

In order to meet the competitive output performance requirements, MGs, equipped with rare-earth PM materials, have widely been introduced and applied in practice and literatures. However, due to the exclusivity of the production and high tendency towards the use of NdFeB PMs, price changing and possibility of not having proper access

The associate editor coordinating the review of this manuscript and approving it for publication was Su Yan.

© 2024 The Authors. This work is licensed under a Creative Commons Attribution-NonCommercial-NoDerivatives 4.0 License.
For more information, see https://creativecommons.org/licenses/by-nc-nd/4.0/

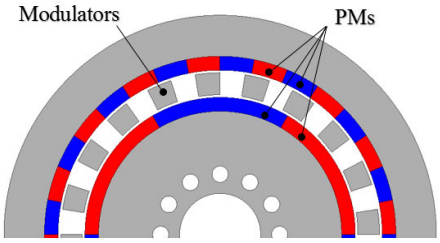


**FIGURE 1.** Conventional radial flux MG.

have created high concerns and risks for their utilization in MGs [16], [17]. Hence, several studies have investigated the use of some alternative topologies with employing non-rare-earth PM materials such as ferrite. Ferrite PM rotors are introduced in form of spoke type to increase torque density through using high amount of PM material and proper flux forming [18]. In addition, to overcome the disadvantage of low residual flux density of ferrite, a geometry design and PM arrangement can be proposed to achieve torque density augmentation and competitive performances with NdFeB PM machines [19], [20].

In order to reduce volume of NdFeB and obtain a comparable performance, an optimal design of PM machines with hybrid ferrite-NdFeB magnets has been proposed [21]. In [22], different rotor configurations with a combination of ferrite and rare-earth magnets has been proposed. The results show that the topology can create a torque competitive with the basic model while using 60% less rare-earth PM volume and lower overall cost. A type of hybrid PM motor introduced in [23], by the combination of NdFeB and ferrite PMs for hybrid electric vehicles [24]. By applying two types of PMs, a hybrid PM motor is proposed in [25] to increase torque density for automotive electric propulsion systems. [26] proposes a PM assisted synchronous reluctance motor with a ferrite magnet. The proposed topology achieves high power density and high efficiency performance with the same power density and an equivalent efficiency as rare-earth PM synchronous motors for hybrid electric vehicles.

This paper proposes a model of coaxial radial flux MG with a hybrid W-shaped interior permanent magnet (HWIPM) and an inner high-speed rotor. The purpose of introducing this structure is to achieve greater maximum output torque density and to reduce cogging torque, while the cost of rare-earth PM consumption decreases compared with conventional IPM MGs. The inner rotor of HWIPM MG will be optimally designed, and two types of rare-earth and ferrite PMs will be placed to maximize the objective function (O.F.). After reviewing and parameterizing the proposed design as well as considering torque density and PM cost, as an O.F., the structure is optimized using genetic algorithm (GA) and particle swarm optimization (PSO) algorithm. At the same time, the results of the optimal proposed HWIPM structure are compared with an optimized conventional MG. Relevant electromagnetic process will be analyzed using the finite element method (FEM), and results of optimal structure simulations will be presented. In this regard, optimization algorithms perform optimizations using 2-D and 3-D FEM software. Finally, in order to validate the results, the experimental results of the optimal HWIPM MG will be presented and compared.

## II. PRINCIPLE OF OPERATION

In conventional MGs, the PMs of inner and outer rotors generate a magnetic field that will be modulated by ferromagnetic modulators to form different harmonics so as to be capable to match with other rotor poles. This will allow the suitable dominant rotational harmonic to be coupled with another PM rotor. The angular velocity of harmonics can be obtained from [27] and [28]:

$$\omega_{m,k} = \frac{mp}{mp + kn_s}\omega_r + \frac{kn_s}{mp + kn_s}\omega_s \tag{1}$$

$$p_{m,k} = |mp + kn_s| \tag{2}$$

$$m = 1, 3, 5, \pm\infty$$

$$k = 0, \pm1, \pm2, \pm3, \pm\infty$$

where $p$ is the number of pole pairs, $n_s$ is the number of modulators, $\omega_r$ is the rotational speed of the PM rotor, and $\omega_s$ is the rotational speed of the modulators. It can be found that $m = 1$ and $k = -1$ leads to the strongest non-principal harmonic, and thus, the number of pole pairs of the third rotor ($p_{m,k}$) should be set as $(n_s - p)$ in order to produce torque in speed of $\omega_{m,k}$ [29], [30]. If outer rotor is kept stationary, the maximum gear ratio can be stated as:

$$G_r = \frac{-n_s}{p_o - n_s} = \frac{n_s}{p_i} \tag{3}$$

where $p_i$, $p_o$ are the numbers of inner and outer rotor pole pairs, respectively.

Four conventional inner rotor structures of radial flux MGs are presented in Fig. 2. As seen, the most popular PM placements are SPM, flat-type IPM, spoke-type IPM, and V-type IPM. In theory, the V-type machines compared with the flat-type structure, can present a greater saliency ratio and lower PM losses, which makes it more appropriate for high-speed constant-power operations. Also, the spoke-type IPM

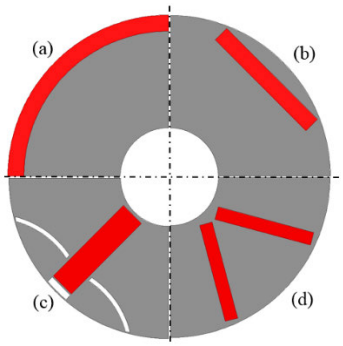


**FIGURE 2.** The conventional structures of inner rotor of coaxial MGs. (a): surface mounted PM, (b): flat-type IPM, (c): spoke type IPM, and (d): V-type IPM.

machines are famous for their intrinsic flux concentration ability. A flat-type IPM MG design, which contributes to the production of reluctance torque, results in higher torque and efficiency combined with magnetic torque from rotor magnets.

In order to overcome the difficulties of rare-earth PMs, alternative MGs, by using non-rare-earth PM materials, will be unavoidable. Due to the low level of torque density in non-rare-earth MGs, a special design and an optimization method will be required to improve MG performances and make it competitive with conventional NdFeB MGs. Thus, a hybrid PM MG can be proposed to enhance torque density. Fig. 3 shows two series-flux and parallel-flux topologies of hybrid PM rotor.

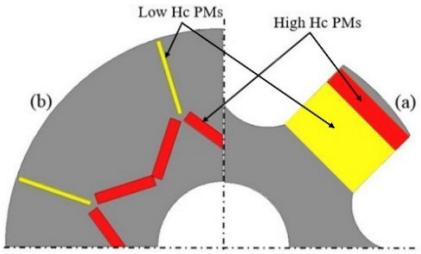


**FIGURE 3.** Typical hybrid PM rotor. (a): series-flux structure, (b): parallel-flux structure.

The series structure of PM placement is shown in Fig.3 (a). Magnetic fields of both PMs are passed through each other. Due to the effect of high-Hc PMs, the low-Hc PMs have a small range of magnetization state [31]. The parallel PM structure is shown in Fig. 3(b). The parallel PM placement structure is unlike the series structure. This type has a large adjustment range of magnetic field [31]. The parallel PM structure has a large adjustment range of magnetic field, and NdFeB PMs can be used to improve the efficiency of the MG. Hence, the proposed structure is based on the parallel PM MG. The use of ferrite PMs reduces flux density, which inevitably leads to a decrease in output torque. In addition, when compared to the SPM structure, the burial of inner rotor PMs results in higher resistance to demagnetization, especially in ferrite PMs, as well as in advantages such as the ability to work at higher temperatures and to increase the stability of the construction model.

## III. ROTOR SHAPE, DEESIGN AND OPTIMIZATION

### A. HWIPM MG

In this paper a parallel HWIPM MG is introduced. The proposal structure of an inner rotor is shown in Fig. 4. Two types of rare-earth (high $H_c$) and non-rare-earth (low $H_c$) PMs are located inside the core. The outer rotor and modulators are the same as that of conventional MGs. The structure of the rotor is presented in such a way that ferrite PM is located in the middle of the pole to reduce the difficulty of PM magnetization. For intrinsic flux concentration ability, flux per pole is generated by five adjacent PMs, four NdFeB PMs, and one ferrite PM. The NdFeB PMs are placed in a V-shaped style symmetrical on both sides of the ferrite PM. The flux barriers are placed at both sides of the ferrite PMs to improve the working point of ferrite PM and to reduce the leakage flux as well as influence of NdFeB PMs.

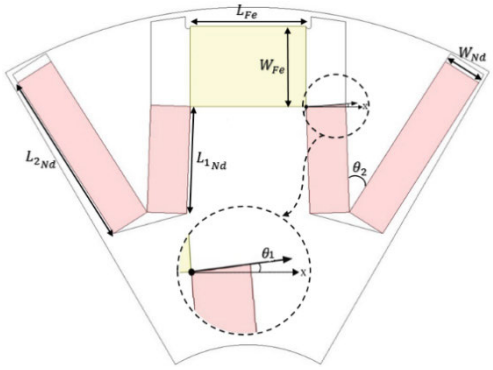


**FIGURE 4.** HWIPM inner rotor topology and corresponding optimization variables.

Optimization variables in HWIPM rotor are shown in Fig. 4. $\theta_1$ is the angle between NdFeB width and X axis. $\theta_2$ is the angle of V-shape NdFeB PMs. $L_{Fe}$ and $W_{Fe}$ are the length and width of ferrite PMs, respectively. $L_{1_{Nd}}$ and $L_{2_{Nd}}$ are the length of inner and outer V-shape NdFeB PMs, respectively. $W_{Nd}$ is the width of NdFeB PMs.

The design parameters of a typical radial flux MG are listed in Table 1. The presented MG has a stationary outer rotor; the middle rotor and the inner rotor act as low- and high-speed rotors, respectively. According to equation (3) the gear ratio will be equal to $G_r$=5.

**TABLE 1.** Design parameters of HPMG.

| Symbol | Quantity | Value |
|---|---|---|
| $p_i$ | Number of high-speed inner rotor pole pairs | 3 |
| $p_o$ | Number of stationary outer rotor pole pairs | 12 |
| $n_s$ | Number of low-speed ferromagnetic pole pieces | 15 |
| $R_{in}$ | Inner radius of high-speed rotor | 15 mm |
| $R_{out}$ | Outer radius of inner high-speed rotor (M400-50A) | 50 mm |
| $l_{gh}$, $l_{gl}$ | Radial length of each air gap | 1 mm |
| $h_{ms}$ | Radial length of ferromagnetic pole pieces | 6 mm |
| $h_{pl}$ | Radial length of stationary PMs | 5 mm |
| $h_{oc}$ | Radial length of stationary outer rotor core | 17 mm |
| - | Slot opening of ferromagnetic pole pieces | 12 deg |
| - | Pole arc to pole pitch ratio of stationary PMs | 1 |
| $B_{r-Nd}$ | Remanence of PMs (NdFeB35) | 1.22 T |
| - | Intrinsic coercivity of PMs (NdFeB35) | 955 kA/m |
| $\rho_{s-Nd}$ | Specific electrical resistance (NdFeB) | 45 $\mu\Omega cm$ |
| $B_{r-Fe}$ | Remanence of PMs (Ferrite C8/Y30H-1) | 385 mT |
| $\rho_{s-Fe}$ | Specific electrical resistance (Ferrite) | 1010 $\mu\Omega cm$ |
| $L$ | Total length of MG | 50 mm |

### B. DESIGN OPTIMIZATION

HWIPM MG optimization will be conducted in a way to achieve a higher O.F.. To introduce an appropriate O.F., maximum torque density transmission, minimum cogging torque, and lowest price of PM according to the ratio of

price coefficients are considered. Given the difference in the price of NdFeB and ferrite PMs, the O.F. will be specified in order to get the highest efficiency from specific volume of PMs. It should be noted that the price per volume unit of the rare-earth PMs is considered as 15 times of ferrite PMs, in this paper [32]. The O.F. can be defined as:

$$O.F. = \frac{T_{d-LS}(kNm/m^3)}{\left(\frac{V_{Ferrite}(m^3)}{15} + V_{NdFeB-HS}(m^3)\right) * \%T_{cogg-LS}} \quad (4)$$

where the $T_{d-Ls}$, $\%T_{cogg-LS}$, $V_{Ferrite}$, and $V_{NdFeB}$ are low speed rotor torque density, low speed cogging torque percentage, the total volume of inner rotor ferrite PMs, and the total volume of inner rotor NdFeB PMs, respectively. The total volume of MG is considered constant (Total MG volume $1.005 \times 10^{-3}\ m^3$)

GA and PSO optimization algorithms integrated with FEM software, is used in this paper. GA operates on three factors: reproduction, crossover, and mutation. The optimization is done by following assumptions: the population size (i.e., 120); maximum number of generation (i.e., 300); crossover probability (i.e., 0.7); and mutation probability (i.e., 0.1). In order to evaluate the output performances of the proposed HWIPM and the conventional flat-type IPM MG, different amounts of inner rotor parameters and correlated restrictions are optimally investigated and designed using a FEM-GA combined method, as shown in Fig. 5. FEM software provides an initial mesh based on ''surface approximation settings''. If needed, the software will improve the condition of the mesh and make it more accurate in more sensitive areas. Initial meshing is possible by the user. Meshing is improved by iterative improvement method in sensitive points with high error density.

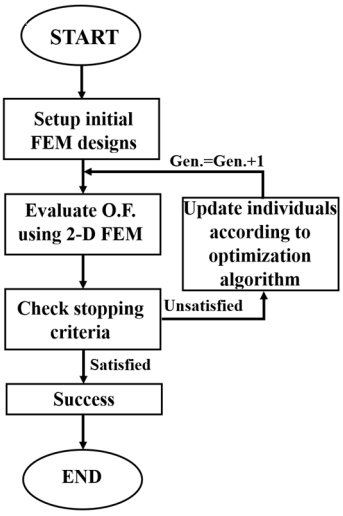


**FIGURE 5.** The optimization flowchart.

In addition to the GA method, particle swarm optimization (PSO) is a well-known efficient population and control parameter-based algorithm for global optimization of different problems. With an adaptable velocity, it is characterized by rapid convergence power and simple evolutionary computation. The standard PSO optimizer begins with a randomly generated population. Each particle in the swarm tends to flow toward the best position that experienced personally in the earlier iterations on one hand, and toward the best position that all particles experienced so far, on the other hand. This leads to good collaborative search capability of the algorithm. Many modifications have been recently proposed to improve the performance and overcome disadvantages of PSO algorithm such as fast convergence of the problem to the local optimum solutions [33], [34]. In this paper the results of GA and PSO optimization will be compared to achieve the best result for maximizing O.F..

## IV. SIMULATION RESULTS

Due to the variables of the ferrite and NdFeB PMs geometry, the magnetic field distribution in air gaps will be controllable, and, thus, O.F. will be changed. Increasing the length and the width of the PMs leads to an increase not only in MMF but also in the reluctance of flux path. Also, by raising the angle $\theta_1$, the NdFeB PMs get closer to the surface of the inner rotor, and by increasing the angle between NdFeB PMs $\theta_2$, the flux orientation and distribution in air gap can be improved, both of which will directly affect O.F. The dimensions of a base typical HWIPM MG have been presented in Table 1. According to Fig. 4, for assuring the precision of the HWIPM rotor design, several restrictions, derived from trial and error, should be considered as:

$$10.4mm \leq L_{Fe} \leq 12.8mm \quad (5)$$
$$7.8mm \leq W_{Fe} \leq 8.6mm \quad (6)$$
$$3.85mm \leq W_{Nd} \leq 4.25mm \quad (7)$$
$$10mm \leq L_{1_{Nd}} \leq 11.2mm \quad (8)$$
$$1\ deg \leq \theta_1 \leq 3.5\ deg \quad (9)$$
$$33.5\ deg \leq \theta_2 \leq 36\ deg \quad (10)$$

The width of the thinnest parts of the core, such as bridges is limited by the mechanical wire cut difficulties. The width of the ferrite PMs affects magnetic field distribution in air gap to compete with NdFeB magnetic field, and distribute the harmonics of flux density in a way that minimum cogging torque and maximum torque transmission can be achieved. Searching for the best amount of $\theta_1$, and $\theta_2$ affects the flux orientation of pole edges to form an optimum magnetic field distribution. Fig. 6 shows the results of the O.F. in HWIPM MG design based on the number of generations in GA and PSO optimization.

The optimization results of HWIPM MG according to Fig. 4 are shown in Table 2. Results show faster convergence in PSO algorithm and relative improvement in optimal O.F. ($18.0927 \times 10^4$ for GA, and $18.6733 \times 10^4$ for PSO). The optimal output performances of HWIPM MG are listed in Table 3. The static and dynamic torque of rotors is shown in Fig. 7 and 8, respectively. Due to the nature of 2-D FEM, the end-effects and leakage fluxes are neglected,

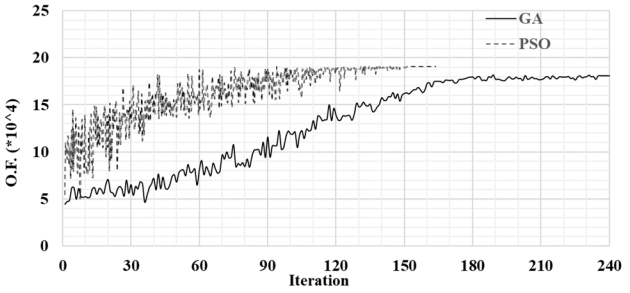


**FIGURE 6.** The optimization of O.F. based on the number of generations using GA and PSO.

**TABLE 2.** Optimal results of HWIPM MG.

| Design variables | Optimum value PSO | GA |
|---|---|---|
| $L_{Fe}$ | *12 mm* | *12 mm* |
| $W_{Fe}$ | *8.3 mm* | *8.2 mm* |
| $W_{Nd}$ | *4.2 mm* | *4.1 mm* |
| $L_{1_{Nd}}$ | *10.8 mm* | *11 mm* |
| $L_{2_{Nd}}$ | *18.5 mm* | *18.5 mm* |
| $\theta_1$ | *2.5 deg* | *2 deg* |
| $\theta_2$ | *36 deg* | *34.5 deg* |

**TABLE 3.** Optimal output performances of HWIPM MG.

| | Middle Rotor (LS) | | | Inner Rotor (HS) | | |
|---|---|---|---|---|---|---|
| | HWIPM MG (GA) | HWIPM MG (PSO) | Conv. flat type MG | HWIPM MG (GA) | HWIPM MG (PSO) | Conv. Flat type MG |
| $T_{avg}$ 2-D FEM (Nm) | *73.2* | *74* | *65* | *14.5* | *14.7* | *13* |
| $T_{avg}$ 3-D FEM (Nm) | *63.89* | *64.6* | *54* | *12.8* | *12.9* | *10.6* |
| $T_{cogg}$ 2-D (%) | *5.4* | *5.2* | *8* | *34.4* | *33* | *53* |
| $T_{cogg}$ 3-D (%) | *4.6* | *4.43* | *7.2* | *32.1* | *31* | *51* |
| *O.F.* | $18.09\times10^4$ | $18.67\times10^4$ | $11.22\times10^4$ | | | |

which leads to an overestimated evaluation of torque transmission [35], [36], [37].

According to Table 3, an optimized HWIPM MG, compared with the existing optimized flat-type IPM structure (with the same general dimensions), presents a better O.F. ($18.67*10^4$ against $11.22*10^4$). This issue is accompanied by the fact that higher torque transmission (1.138 times) and lower level of cogging torque (0.65 times) can be achieved with a slight increase of about 1.03 times in inner rotor PM usage of HWIPM MG, in contrast to the flat-type IPM MG.

The magnetic potential lines and flux density distribution in 2-D and 3-D FEM simulations are shown in Fig. 9-a and 9-b, respectively. The magnetic flux density distribution between adjacent NdFeB PMs is higher than other parts of

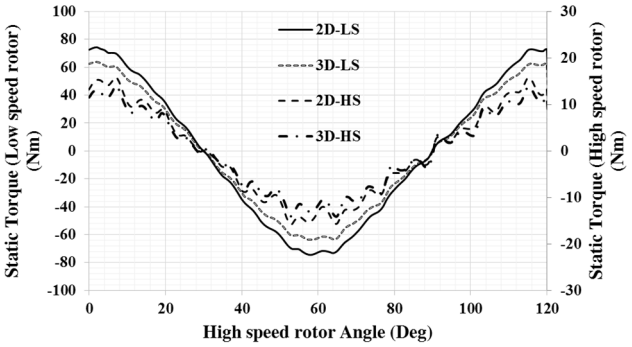


**FIGURE 7.** Static Torque of middle rotor (LS) and inner rotor (HS) of optimal HWIPM MG using 2-D and 3-D FEM.

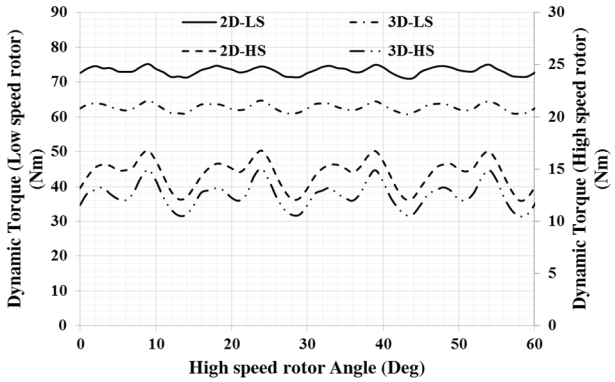


**FIGURE 8.** Dynamic Torque of middle rotor (LS) and inner rotor (HS) of optimal HWIPM MG using 2-D and 3-D FEM.

the rotor. Also, at the sharp edges of the inner rotor and modulator, the flux density is high and may instantaneously cause momentary saturation [27].

The von Mises stress on the inner rotor is simulated by a centrifugal force analysis using Ansys 2021 R.2. Fig. 10 shows the maximum Mises stress generated in different rotor speeds. The yield strength of the core (M400-50A) is about 350 MPa.

It can be seen that a maximum acceptable speed of about 12500 rpm can be a safe range speed, and working in higher speeds will be limited by this stress. Fig. 11 shows the graphical distribution of Mises stress and the total deformation distribution of the inner core in a maximum acceptable speed. The Mises stress concentrates in the ends of barriers. Hence, high speed applications (over 12500 rpm) can be a challenge and a limiting factor.

## V. EXPERIMENTAL VALIDATION

In order to evaluate the accuracy of FEM and optimization results and the technical feasibility of the proposed structure, the optimal HWIPM MG is manufactured according to the results of Table 2. The fabricated optimal inner rotor is shown in Fig. 12.

In Fig. 13, the test bench shows a primary mover as a high-speed side, a torque transducer, and a magnetic powder brake

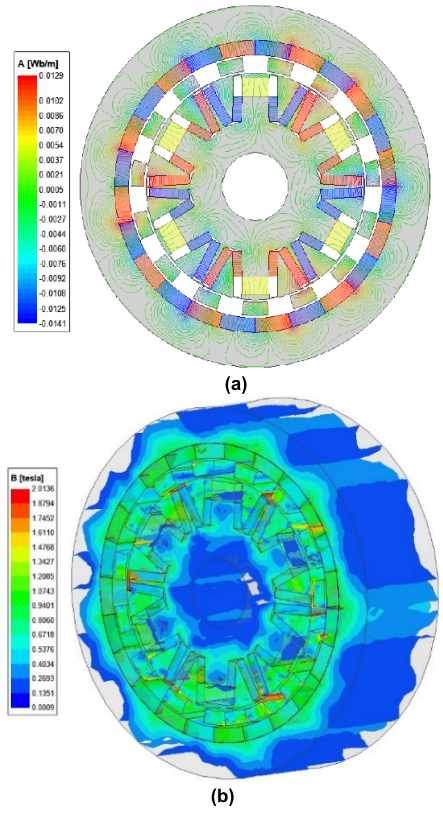


**FIGURE 9.** (a): 2-D magnetic potential lines distribution (b): 3-D magnetic flux density distribution.

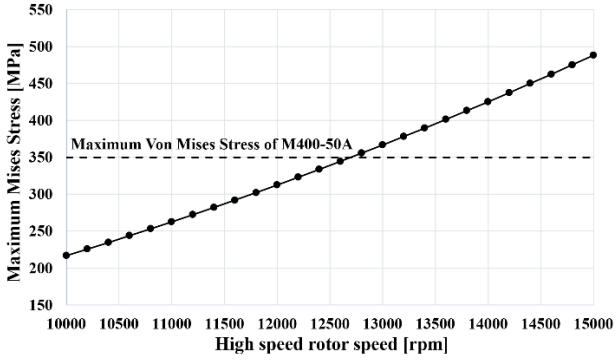


**FIGURE 10.** Maximum von Mises stress of the inner core based on the speed of HS rotor.

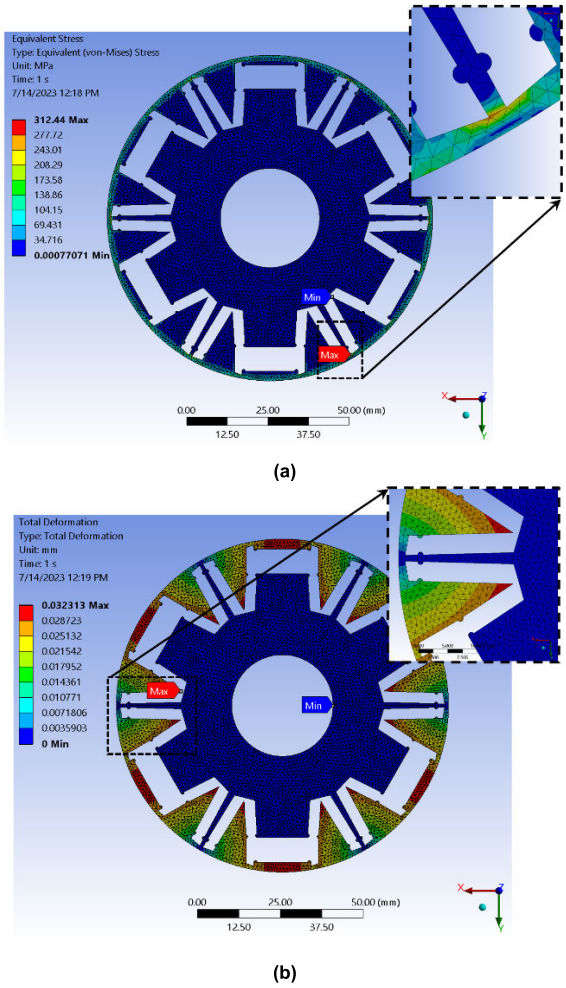


**FIGURE 11.** Mechanical analysis of FB rotor in 12500 rpm (a) Mises stress distribution and (b) total deformation distribution.

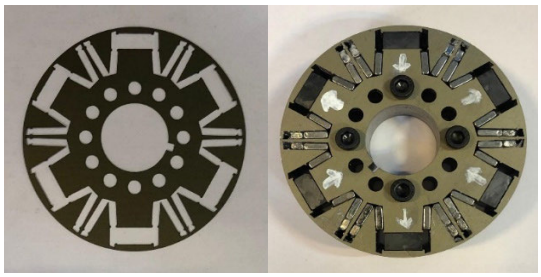


**FIGURE 12.** HWIPM inner rotor (a): lamination core and (b): inner rotor by PM placement.

equipped with an interior torque transducer as a low-speed side. The output static torque is measured as the function of a high-speed rotor angle through locking the modulator low-speed rotor and the rotating of the input shaft. The resultant static torque measurements are shown in Fig. 14.

According to the Fig. 14, a maximum torque of 55 Nm can be achieved on low-speed shaft. The experimental torque in Fig. 14 is very close to 3-D FEM results, with a difference of about 13.9%, which can partly be caused by manufacturing imperfections and measurement errors. A part of this deviation is caused by the difference in the core characteristics applied in FEM software and inaccurate dimensions of PMs. Another source of discrepancy between the experimental and simulated results originates from the test setup. Due to the finite stiffness of couplings and bearings, the rotor may not have completely been fixed. The experimental low-speed dynamic torque, as a function of time, is shown in Fig. 15. As it can be seen, the torque ripple is higher than the expectation (17.5 Nm, 31.8% at peak torque), which can be caused by

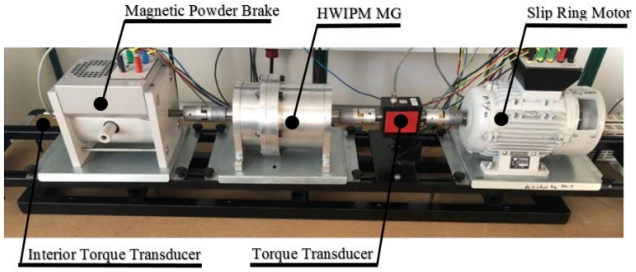


**FIGURE 13.** Fabricated optimal HWIPM MG.

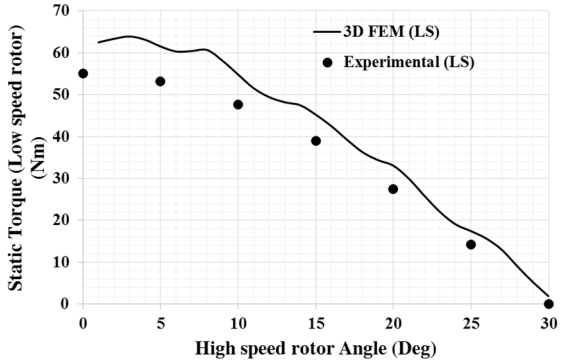


**FIGURE 14.** Static LS torque of experimental and 3-D FEM simulations.

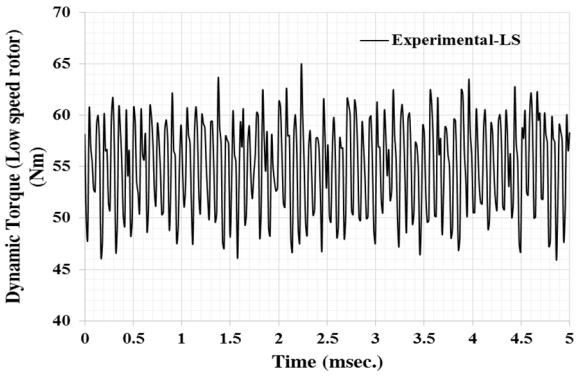


**FIGURE 15.** Experimental dynamic torque of LS rotor (at 800rpm).

unwanted mechanical vibrations in the setup or an eccentric air gap.

The effect of load change on the dynamic behavior of torque is shown in Figure 15. In this section, the load torque increases from half to the final value. The behavior of the transient state shows that the torque fluctuations are damped for a significant period of time and in this transient state the torque may exceed the maximum value, in which case in the next round, the rotor tries to establish magnetic engagement and power transmission by reducing the torque. The use of damping rods can be effective in reducing these fluctuations and transient time [38].

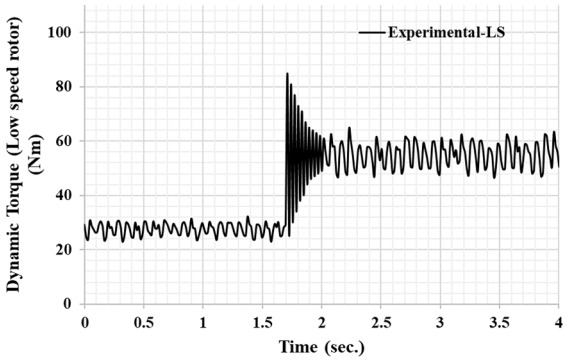


**FIGURE 16.** Effect of load change in transient dynamic torque.

## VI. CONCLUSION

This paper proposes a coaxial MG with HWIPM inner high-speed rotor. A GA and PSO optimization method is applied to optimize the design of the inner rotor structure of HWIPM MG. The results show relatively better performance of PSO algorithm compared to GA. Compared with conventional flat type PM structure, the results of proposed structure present a better O.F. in form of higher torque transmission (1.138 times) and lower level of cogging torque (0.65 times) with a slight increase of about 1.03 times in the inner rotor PM usage. By combining both NdFeB PM and ferrite PM materials in a high-speed rotor, the HWIPM MG can provide not only improved output performances but also lower PM cost at the same output performance. Both the simulation and experimental results confirm the advantages of the proposed HWIPM MG and of the design optimization method.

## REFERENCES

[1] E. Gouda, S. Mezani, L. Baghli, and A. Rezzoug, "Comparative study between mechanical and magnetic planetary gears," *IEEE Trans. Magn.*, vol. 47, no. 2, pp. 439–450, Feb. 2011.

[2] P. O. Rasmussen, T. O. Andersen, F. T. Jorgensen, and O. Nielsen, "Development of a high-performance magnetic gear," *IEEE Trans. Ind. Appl.*, vol. 41, no. 3, pp. 764–770, May 2005.

[3] K. Atallah and D. Howe, "A novel high-performance magnetic gear," *IEEE Trans. Magn.*, vol. 37, no. 4, pp. 2844–2846, Jul. 2001.

[4] L. Jing, W. Tang, T. Wang, T. Ben, and R. Qu, "Performance analysis of magnetically geared permanent magnet brushless motor for hybrid electric vehicles," *IEEE Trans. Transport. Electrific.*, vol. 8, no. 2, pp. 2874–2883, Jun. 2022.

[5] M. Filippini, R. Torchio, P. Alotto, E. Bonisoli, L. Dimauro, and M. Repetto, "A new class of devices: Magnetic gear differentials for vehicle drivetrains," *IEEE Trans. Transport. Electrific.*, vol. 9, no. 2, pp. 2382–2397, Jun. 2023.

[6] S. Xie et al., "A magnetic-geared machine with improved magnetic circuit symmetry for hybrid electric vehicle applications," *IEEE Trans. Transport. Electrific.*, vol. 10, no. 1, pp. 2170–2182, Mar. 2023.

[7] K. Tsurumoto, "Generating mechanism of magnetic force in meshing area of magnetic gear using permanent magnet," *IEEE Transl. J. Magn. Jpn.*, vol. 6, no. 6, pp. 531–536, Jun. 1991.

[8] D. E. Hesmondhalgh and D. Tipping, "A multielement magnetic gear," *IEE Proc. B, Electr. Power Appl.*, vol. 127, no. 3, pp. 129–138, 1980.

[9] K. Tsurumoto and S. Kikuchi, "A new magnetic gear using permanent magnet," *IEEE Trans. Magn.*, vol. MAG-23, no. 5, pp. 3622–3624, Sep. 1987.

[10] K. Ikuta, S. Makita, and S. Arimoto, "Non-contact magnetic gear for micro transmission mechanism," in *Proc. IEEE Micro Electro Mech. Syst.*, Jan. 1991, pp. 125–130.
[11] Y. D. Yao, D. R. Huang, S. M. Lin, and S. J. Wang, "Theoretical computations of the magnetic coupling between magnetic gears," *IEEE Trans. Magn.*, vol. 32, no. 3, pp. 710–713, May 1996.
[12] F. Parasiliti, M. Villani, S. Lucidi, and F. Rinaldi, "Finite-element-based multiobjective design optimization procedure of interior permanent magnet synchronous motors for wide constant-power region operation," *IEEE Trans. Ind. Electron.*, vol. 59, no. 6, pp. 2503–2514, Jun. 2012.
[13] F. Parasiliti and P. Poffet, "A model for saturation effects in high-field permanent magnet synchronous motors," *IEEE Power Eng. Rev.*, vol. 9, no. 9, pp. 50–51, Sep. 1989.
[14] P. Zhang, D. M. Ionel, and N. A. Demerdash, "Morphing parametric modeling and design optimization of spoke and V-type permanent magnet machines by combined design of experiments and differential evolution algorithms," in *Proc. IEEE Energy Convers. Congr. Expo.*, Sep. 2013, pp. 5056–5063.
[15] H. Zhao, C. Liu, Z. Dong, R. Huang, and X. Li, "Design and optimization of a magnetic-geared direct-drive machine with V-shaped permanent magnets for ship propulsion," *IEEE Trans. Transport. Electrific.*, vol. 8, no. 2, pp. 1619–1633, Jun. 2022.
[16] G. Pellegrino, A. Vagati, P. Guglielmi, and B. Boazzo, "Performance comparison between surface-mounted and interior PM motor drives for electric vehicle application," *IEEE Trans. Ind. Electron.*, vol. 59, no. 2, pp. 803–811, Feb. 2012.
[17] S.-U. Chung, J.-W. Kim, Y.-D. Chun, B.-C. Woo, and D.-K. Hong, "Fractional slot concentrated winding PMSM with consequent pole rotor for a low-speed direct drive: Reduction of rare Earth permanent magnet," *IEEE Trans. Energy Convers.*, vol. 30, no. 1, pp. 103–109, Mar. 2015.
[18] S.-I. Kim, J. Cho, S. Park, T. Park, and S. Lim, "Characteristics comparison of a conventional and modified spoke-type ferrite magnet motor for traction drives of low-speed electric vehicles," *IEEE Trans. Ind. Appl.*, vol. 49, no. 6, pp. 2516–2523, Nov. 2013.
[19] W. Zhao, T. A. Lipo, and B.-I. Kwon, "Comparative study on novel dual stator radial flux and axial flux permanent magnet motors with ferrite magnets for traction application," *IEEE Trans. Magn.*, vol. 50, no. 11, pp. 1–4, Nov. 2014.
[20] Y. Zhou, Y. Chen, and J.-X. Shen, "Analysis and improvement of a hybrid permanent-magnet memory motor," *IEEE Trans. Energy Convers.*, vol. 31, no. 3, pp. 915–923, Sep. 2016.
[21] C.-L. Jeong, Y.-K. Kim, and J. Hur, "Optimized design of PMSM with hybrid-type permanent magnet for improving performance and reliability," *IEEE Trans. Ind. Appl.*, vol. 55, no. 5, pp. 4692–4701, Sep. 2019.
[22] Q. Ma, A. El-Refaie, and B. Lequesne, "Low-cost interior permanent magnet machine with multiple magnet types," *IEEE Trans. Ind. Appl.*, vol. 56, no. 2, pp. 1452–1463, Mar. 2020.
[23] A. S. Al-Adsani and O. Beik, "Design of a multiphase hybrid permanent magnet generator for series hybrid EV," *IEEE Trans. Energy Convers.*, vol. 33, no. 3, pp. 1499–1507, Sep. 2018.
[24] I. Boldea, L. N. Tutelea, L. Parsa, and D. Dorrell, "Automotive electric propulsion systems with reduced or no permanent magnets: An overview," *IEEE Trans. Ind. Electron.*, vol. 61, no. 10, pp. 5696–5711, Oct. 2014.
[25] Q. Chen, G. Liu, W. Zhao, M. Shao, and Z. Liu, "Design and analysis of the new high-reliability motors with hybrid permanent magnet material," *IEEE Trans. Magn.*, vol. 50, no. 12, pp. 1–10, Dec. 2014.
[26] M. Obata, S. Morimoto, M. Sanada, and Y. Inoue, "Performance of PMASynRM with ferrite magnets for EV/HEV applications considering productivity," *IEEE Trans. Ind. Appl.*, vol. 50, no. 4, pp. 2427–2435, Jul. 2014.
[27] G. Bacco and N. Bianchi, "Design criteria of flux-barriers in synchronous reluctance machines," *IEEE Trans. Ind. Appl.*, vol. 55, no. 3, pp. 2490–2498, May 2019.
[28] S. Yammine, C. Henaux, M. Fadel, S. Desharnais, and L. Calégari, "Synchronous reluctance machine flux barrier design based on the flux line patterns in a solid rotor," in *Proc. Int. Conf. Electr. Mach. (ICEM)*, Sep. 2014, pp. 297–302.
[29] K. Jenney and S. Pakdelian, "Magnetic design aspects of the trans-rotary magnetic gear using quasi-Halbach arrays," *IEEE Trans. Ind. Electron.*, vol. 67, no. 11, pp. 9582–9592, Nov. 2020.
[30] S. A. Afsari Kashani, "Rotor pole design of radial flux magnetic gear for reduction of flux density harmonics and cogging torque," *IEEE Trans. Appl. Supercond.*, vol. 29, no. 8, pp. 1–8, Dec. 2019.
[31] Y. Hu, B. Chen, Y. Xiao, X. Li, Z. Zhang, J. Shi, and L. Li, "Research and design on reducing the difficulty of magnetization of a hybrid permanent magnet memory motor," *IEEE Trans. Energy Convers.*, vol. 35, no. 3, pp. 1421–1431, Sep. 2020.
[32] X. Zhu, W. Wu, L. Quan, Z. Xiang, and W. Gu, "Design and multi-objective stratified optimization of a less-rare-earth hybrid permanent magnets motor with high torque density and low cost," *IEEE Trans. Energy Convers.*, vol. 34, no. 3, pp. 1178–1189, Sep. 2019.
[33] M. Ghasemi, E. Akbari, A. Rahimnejad, S. E. Razavi, S. Ghavidel, and L. Li, "Phasor particle swarm optimization: A simple and efficient variant of PSO," *Soft Comput.*, vol. 23, no. 19, pp. 9701–9718, Oct. 2019.
[34] M. Ghasemi, J. Aghaei, and M. Hadipour, "New self-organising hierarchical PSO with jumping time-varying acceleration coefficients," *Electron. Lett.*, vol. 53, no. 20, pp. 1360–1362, Sep. 2017.
[35] B. Dianati, H. Heydari, and S. A. Afsari, "Analytical computation of air-gap magnetic field in a viable superconductive magnetic gear," *IEEE Trans. Appl. Supercond.*, vol. 26, no. 6, pp. 1–12, Sep. 2016.
[36] T. J. E. Miller, "Optimal design of switched reluctance motors," *IEEE Trans. Ind. Electron.*, vol. 49, no. 1, pp. 15–27, Feb. 2002.
[37] S. A. A. Kashani, "Design and optimization of coaxial reluctance magnetic gear with different rotor topologies," *IEEE Trans. Ind. Electron.*, vol. 69, no. 1, pp. 101–109, Jan. 2022.
[38] N. W. Frank, S. Pakdelian, and H. A. Toliyat, "Passive suppression of transient oscillations in the concentric planetary magnetic gear," *IEEE Trans. Energy Convers.*, vol. 26, no. 3, pp. 933–939, Sep. 2011.

**MOHAMMAD AMIN MASOUDI** was born in Esfahan, Isfahan, Iran, in 1994. He received the B.S. degree in electrical engineering (electrical power engineering) from Islamic Azad University, Najafabad, Iran, in 2017, and the M.Sc. degree in electrical power engineering from the University of Kashan, Kashan, Iran, in 2022. His research interests include electrical machine design, power engineering, renewable energy systems, magnetic gears, finite-element-method-based simulation techniques, and optimization methods.

**SEYED AHMADREZA AFSARI** was born in Kashan, Iran, in 1994. He received the B.S. degree in electrical engineering (electrical power engineering) from the K. N. Toosi University of Technology, Tehran, Iran, in 2007, the M.Sc. degree in electrical power engineering from the University of Kashan, Kashan, in 2010, and the Ph.D. degree in electrical machine design from Iran University of Science and Technology (IUST), Tehran, in 2016. Following graduation, he joined the University of Kashan, Kashan, as an Assistant Professor with the Electrical Power Group, and also appointed as the Director of the Modern Electrical Machine and Magnetic Materials Laboratory. His research interests include novel electrical machine design, magnetic gears, analytical methods, finite-element-method-based simulation techniques, optimization methods, and applied superconductors in power systems.